\$ SUPER

Contents lists available at ScienceDirect

# Electrochimica Acta

journal homepage: www.journals.elsevier.com/electrochimica-acta





# Measurement of neuropeptide Y in aptamer-modified planar electrodes

Luis López <sup>a</sup>, Lyza M. Martínez <sup>b</sup>, Jaileen R. Caicedo <sup>a</sup>, Lauren Fernández-Vega <sup>b,c</sup>, Lisandro Cunci <sup>a,\*</sup>

- a Department of Chemistry, University of Puerto Rico Rio Piedras, 17 Ave Universidad Ste 1701, San Juan, Puerto Rico 00931, United States
- b Department of Chemistry, Universidad Ana G. Méndez Gurabo, Carr. 189, Km 3.3, Gurabo, Puerto Rico 00778, United States
- <sup>c</sup> Department of Chemistry, Universidad Ana G. Méndez Cupey, 1399 Ave Ana G Mendez, Cupey, Puerto Rico 00925, United States

### ARTICLE INFO

# Keywords: Neuropeptide Y Electrochemical impedance spectroscopy Biosensing Single layer adsorption Langmuir isotherm

#### ABSTRACT

Electrochemical impedance spectroscopy (EIS) is a powerful technique for studying the interaction at electrode/solution interfaces. The adoption of EIS for obtaining analytical signals in biosensors based on aptamers is gaining popularity because of its advantageous characteristics for molecular recognition. Neuropeptide Y (NPY), the most abundant neuropeptide in the body, plays a crucial role with its stress-relieving properties. Quantitative measurement of NPY is imperative for understanding its role in these and other biological processes. Although aptamer-modified electrodes for NPY detection using EIS present a promising alternative, the correlation between the data obtained and the adsorption process on the electrodes is not fully understood. Various studies utilize the change in charge transfer resistance when employing an active redox label. In contrast, label-free measurement relies on changes in capacitance. To address these challenges, we focused on the interaction between aptamer-modified planar electrodes and their target, NPY. We proposed utilizing  $-\omega^*Z_{imag}$  as the analytical signal, which facilitated the analysis of the adsorption process using an analogous Langmuri isotherm equation. This approach differs from implantable microelectrodes, which adhere to the Freundlich adsorption isotherm. Notably, our method obviates the need for a redox label and enables the detection of NPY at concentrations as low as 20 pg/mL. This methodology demonstrated exceptional selectivity, exhibiting a signal difference of over 20-to-1 against potential interfering molecules.

### 1. Introduction

Most biological sensors monitor the electron transfer kinetics of specific molecular targets. Aptamer-based electrochemical sensors exemplify this by utilizing a target-specific aptamer, which is covalently modified with or without a redox reporter. [1–3] Binding of a target to the surface of an electrode modified with label-modified aptamers can induce a conformational change in the aptamer, consequently affecting the electron transfer correlated to the target's concentration. [4] Sensors leveraging changes in electron transfer rate due to binding typically employ voltammetric techniques [5,6] to monitor the sensor's response to the target. [7,8] Electrochemical impedance spectroscopy (EIS) provides insights not only into the target's concentration [9] but also its adsorption on the surface. EIS measures changes in interfacial surface properties by applying sinusoidally oscillating alternating current [10], where changes in these properties can indicate target binding through electrode capacitance changes. [11,12]

Neuropeptides, integral to the transmission and modulation of neurological signals, [13] require sensitive detection methods with high time resolution. They are often released alongside other neurotransmitters, [14] necessitating systems capable of selective measurement while filtering out signals from other neurotransmitters. Neuropeptide Y (NPY), a key neuropeptide in numerous biological applications, including stress response [15] and appetite regulation, [16] has been implicated in various disorders, such as post-traumatic stress disorder when dysregulated. [17] Hence, developing accurate and reliable methods for NPY detection and understanding the processes in its biosensors are crucial. Conventional techniques for NPY detection include microdialysis coupled with mass spectrometry [18] and colorimetry. [19] Additionally, various molecular recognition elements like antibodies [20,21] have been employed for its measurement. In a recent study, J. M. Seibold and colleagues introduced a novel application of aptamer-modified microelectrodes for the dynamic measurement of NPY, presenting the possibility of achieving superior spatial and

E-mail address: lisandro.cunci@upr.edu (L. Cunci).

 $<sup>^{\</sup>ast}$  Corresponding author.

temporal resolution. [22] The researchers demonstrated precise measurements of NPY in serum; however, the technique's lower limit was constrained to 20 nM (4704 pg/mL). Moreover, our group recently published the first carbon fiber microelectrode sensitive to different NPY concentrations as low as 50 ng/mL based on molecularly imprinted polypyrrole. [23] All these sensors, however, are based on microelectrodes for implanted biosensors. In this paper, however, thanks to the use of planar Au electrodes with EIS, we were able to measure NPY as low as 20 pg/mL.

EIS is a popular technique in the development of electrochemical aptamer biosensors. [24] Depending on the applied frequencies, it can be linked with the adsorption process, allowing for monitoring of target interaction with the electrode surface. [9,25] Despite the advantages of EIS in biosensing, its application in aptamer biosensor development has been limited. [7,26] Numerous aptamer-based biosensors demonstrate that aptamers are viable alternatives to antibodies [27] as detection elements due to their stability, ease of synthesis, cost-effectiveness, and potential for labeling. [28] Their small size also makes them suitable for tissue studies. Combining EIS with aptamers can effectively develop biosensors for various targets [29–31] in real samples, improving selectivity through specific potentials and frequencies. [32] NPY detection using EIS represents a promising approach for developing sensitive and selective NPY detection assays.

In this study, we developed an aptamer-modified biosensor to detect NPY using planar electrodes. The aptamer was immobilized on the surface of a gold (Au) electrode using a standard self-assembled monolayer (SAM) formation protocol. EIS was employed to monitor NPY binding to the aptamer-modified electrode. We examined NPY adsorption at varying concentrations on a highly planar surface to understand the differences in adsorption behavior compared to previous studies involving microelectrodes and to enhance biosensing applications. [33, 34] Our results indicate a significant change in the electrodes' capacitance upon NPY binding, even in the picogram per milliliter range. The biosensor exhibited high selectivity for NPY without substantial electrochemical interference from other biomolecules like dopamine (DA), norepinephrine (NE), and serotonin (5-HT) at concentrations 20 times higher.

## 2. Methods

## 2.1. Au electrode fabrication

The Au electrodes were fabricated at the Conte Nanotechnology Cleanroom Laboratory, a part of the Center of Hierarchical Manufacturing at the University of Massachusetts, Amherst. For this purpose, 500  $\mu m$  thick, single-side polished silicon wafers were used. These wafers were coated with a layer of approximately 200 nm SiO2 and deposited using plasma-enhanced chemical vapor deposition for electrical isolation. Subsequently, two layers, consisting of 5 nm of titanium (Ti) and 150 nm of Au, were deposited using a CHA SE-600 electron beam evaporator. The surface of the Au electrodes was obtained from the deposition process.

# 2.2. Physical characterization

For atomic force microscopy (AFM) imaging, an ezAFM+ AQUA from Nanomagnetics Instruments was employed. Standard silicon cantilevers were used, and the instrument was automatically calibrated before each sample. AFM images were acquired in water. The changes in the composition of the electrode surfaces post-fabrication were analyzed using scanning electron microscopy (SEM) coupled with energy-dispersive X-ray spectroscopy (EDS). A JSM-6010LA model from JEOL was used for SEM-EDS.

### 2.3. Electrochemical measurements

All electrochemical measurements were conducted using a threeelectrode cell comprising the modified Au electrode as the working electrode, a platinum wire as the counter electrode, and an Ag|AgCl reference electrode filled with a 3 M KCl solution. Electrochemical measurements were performed using a Reference 600+ Gamry potentiostat, and all data were collected using Gamry Instruments Framework software. All potentials in this work are reported versus Ag|AgCl. EIS was conducted with an amplitude of 10 mV, an initial frequency of 1 MHz, and a final frequency of 10 Hz. Data analysis was carried out using Gamry Echem and OriginPro 2023b software. The electrochemical characterization of the Au electrodes was performed in artificial cerebrospinal fluid (aCSF) at pH 7.4. The solution was prepared with 150 mM NaCl, 1.4 mM CaCl<sub>2</sub>, 3 mM KCl, 0.8 mM MgCl<sub>2</sub>, 0.8 mM Na<sub>2</sub>H-PO<sub>4</sub>·7H<sub>2</sub>O, 0.17 mM NaH<sub>2</sub>PO<sub>4</sub>·2H<sub>2</sub>O, and 0.5 M Tris in nanopure water (18.2  $M\Omega$ ). Human serum albumin (HSA) was used to study the biofouling of the electrodes by mixing 5 g of HSA (Sigma-Aldrich) in 50 ml of aCSF. NPY (GenScript), along with DA, NE, and 5-HT (Sigma-Aldrich), were diluted in aCSF to create standard solutions. The electrochemical cell used had a volume of 15 mL. After adding aliquots of NPY, DA, NE, or 5-HT, the cell was stirred for 1 min and left until the solution stabilized to mitigate convection effects.

### 2.4. Aptamer immobilization

The Au electrodes were modified by incubating them overnight at room temperature in 1.0  $\mu M$  solutions of a single-stranded DNA aptamer (5'-S-S-C6-AGC AGC ACA GAG GTC AGA TGC AAA CCA CAG CCT GAG TGG TTA GCG TAT GTC ATT TAC GGA CCT ATG CGT GCT ACC GTG AA-3') purchased to Integrated DNA Technologies. The disulfide bonds at the 5'-end were reduced through a 2 hrs. reaction with 200  $\mu M$  tris(2-carboxyethyl)phosphine (TCEP). The modified electrodes were then immersed in a 5 mM 6-mercapto-1-hexanol solution in aCSF overnight and shielded from light. Before measurements, the electrodes were rinsed with deionized (DI) water.

### 3. Results and discussion

### 3.1. Aptamer self-assembled monolayer deposition

Aptamer (Apt) immobilization was conducted using a SAM on Aucoated silicon wafers. To modify the surface, Apts with a disulfide bond at the 5' end (Apt-S-S-Apt) were employed. Before surface modification, this disulfide bond was reduced using TCEP as the reducing agent. Given that thiols directly react with Au surfaces, the interaction of the reduced Apt with the electrode facilitates the formation of an Au-S bond, resulting in Apt-modified Au-coated silicon wafer electrodes. Literature indicates that this reaction initially involves physisorption, where the thiol group adsorbs onto the Au surface. [35,36] Subsequently, a chemisorption process occurs, involving the cleavage of the S–H bond. The final step in obtaining Apt-modified Au silicon wafer electrodes involves the formation of the Au–S bond between the Apt and the Au surface, resulting from the deprotonation of thiols. [37] Fig. 1 illustrates the schematic of the Apt modification on the Au-coated planar electrodes. [35]

# 3.2. Electrochemical and surface characterization of aptamer-modified AU electrodes

AFM, EDS, cyclic voltammetry (CV), and EIS were employed to analyze the NPY aptamer-modified Au electrodes. Tapping mode-AFM was used to assess the Au coverage at the electrode surface postfabrication. The Au surface topography exhibited a characteristic pattern on the surface of the Au-coated silicon wafers (Fig. 2A), confirming the Au deposition by electron beam evaporation at the electrode

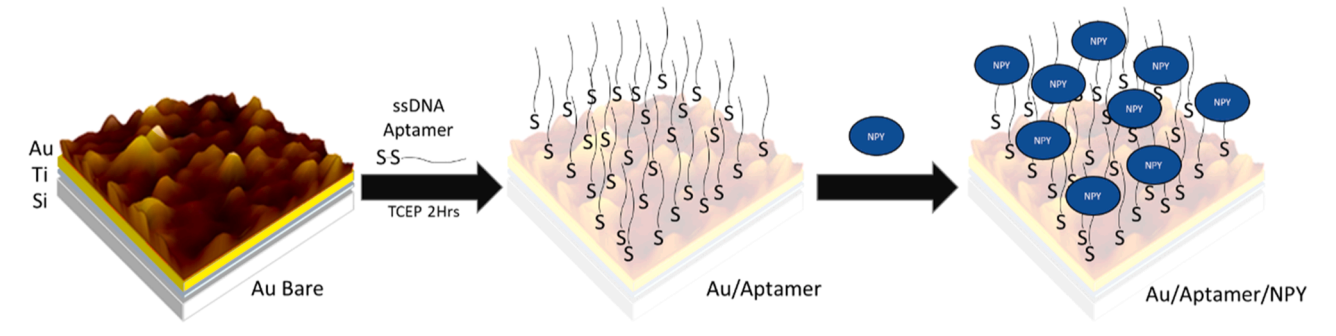


Fig. 1. Schematic for modification of the Au surface of the working electrode with ssDNA-aptamer specific for NPY. The binding of NPY to the aptamer-modified electrode shows higher adsorption compared to DA, NE, and HT.

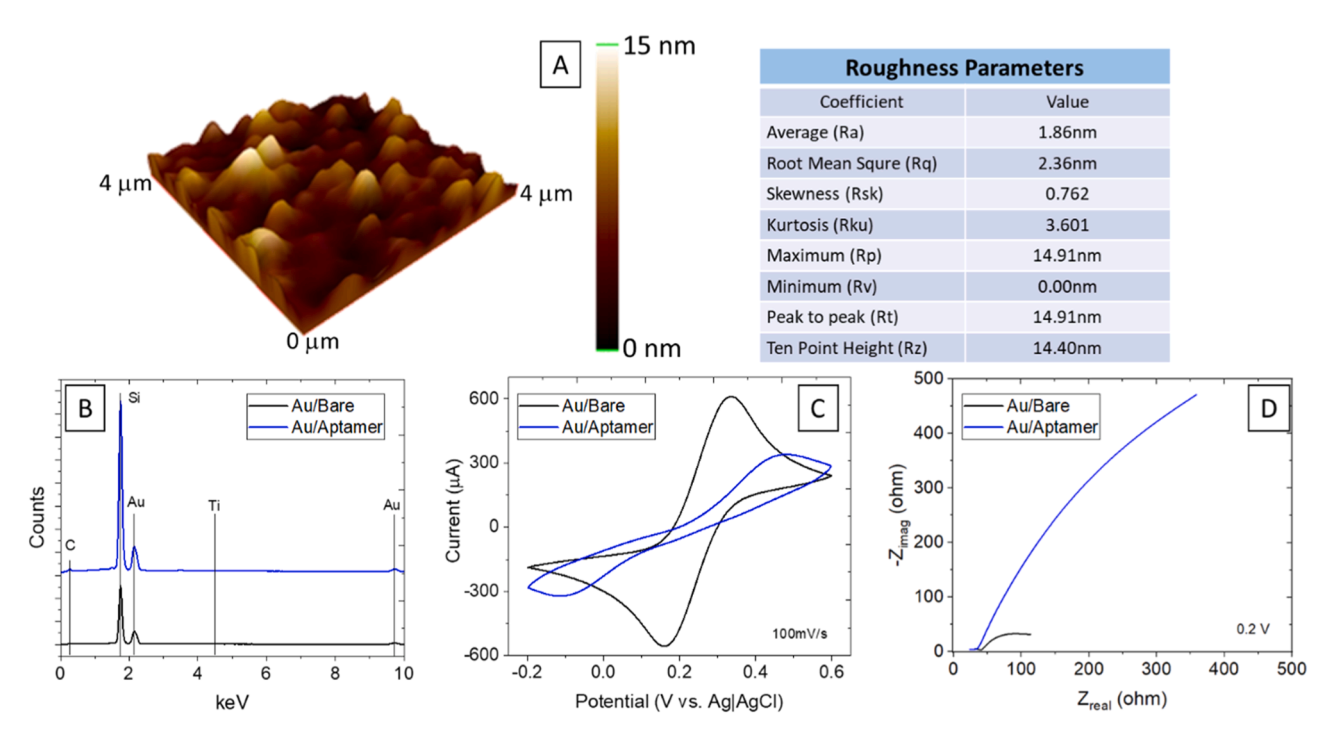


Fig. 2. (A) AFM image of Bare Au Electrode. (B) EDS of the surface-deposited Au. Electrochemical characterization of the aptamer-modified Au electrodes using (C) CV and (D) Nyquist plot.

surface. [38,39] Electron beam evaporation achieved a highly planar surface with an average roughness of 1.86 nm and a peak-to-peak distance of 14.91 nm. Surface modification with an ssDNA Apt of 80 bases, including a 6-carbon chain and thiol end, is expected to yield a length exceeding 55 nm, based on the average size per base calculated by Q. Chi et al. [40] of 0.676 nm and a width of less than 5 nm. [41,42] Considering the Apt's size relative to the average surface roughness of 1.86 nm, the surface is anticipated to function as a planar electrode where a single layer of aptamers binds with uniform energy at each site. Furthermore, considering the longest side of NPY (LYS 4 – TYR 36) is approximately 5 nm, it is anticipated that the binding should not exert a significant impact on the electrochemical behavior of the surface functioning as a planar electrode.

EDS (Fig. 2B) confirmed the presence of two distinctive peaks at 2.120 and 9.712 keV, corresponding to Au on the surface (150 nm). A smaller peak for Ti at 4.530 keV, utilized as an adhesion layer (5 nm) to prevent Au film detachment, and the silicon peak at 1.750 keV, attributable to the silicon wafer substrate, were also observed. CV was conducted to ascertain the electrochemical behavior alterations pre- and post-aptamer modification (Fig. 2C). The CV analysis was performed at a scan rate of 100 mV/s in  $5 \text{ mM K}_3\text{Fe}(\text{CN})_6/\text{K}_4\text{Fe}(\text{CN})_6$  in 0.1 M KCl

vs. Ag|AgCl. Post-Apt addition, a slowdown in kinetics was noted, characterized by the widening gap between the anodic and cathodic current peaks. This variation between the bare and the aptamer-modified electrode substantiated the aptamer surface modification on the Au-coated silicon wafers. Although short ssDNA chains may enhance kinetics on Au electrode surfaces, [39] long aptamers on planar surfaces are likely to hinder electron transfer, evidenced by the loss of system reversibility even at 100 mV/s. [43]

EIS is a technique employed to detect changes in electrode interfacial properties, providing insights into the interactions of analytes with their corresponding probing molecules immobilized on electrode surfaces. [44,45] Fig. 2D presents the Nyquist plot for both the bare and Apt-modified Au electrodes at a potential of 0.2 V vs. Ag|AgCl. Following Apt modification, a heightened charge transfer resistance was anticipated, in line with the previously observed loss of electrochemical reversibility in CV. This increase in electron transfer resistance can be attributed to the surface modification by a long aptamer, which obstructs the surface and complicates electron transfer between the electrode and the solution. [46] These findings suggest the formation of a densely packed single layer of aptamers on the planar Au electrode.

### 3.3. Electrochemical impedance analysis of NPY

EIS has been extensively utilized to examine biomolecule adsorption on electrode surfaces, largely due to its insights into surface characteristics via double-layer capacitance analysis. [47] Previous studies have demonstrated that the adsorption of diverse molecules, such as DA on carbon fiber [33] and NPY on platinum [34] microelectrodes, conforms to the Freundlich isotherm. This section aims to investigate the adsorption of NPY at varying concentrations on a highly planar surface to discern differences in adsorption behaviors compared to carbon fiber and metal microelectrodes in biosensing applications.

According to N. K. Mintha Churcer et al. [48] and K. Ensing et al. [49] the isoelectric point of NPY is 7.9, and according to L. Thomas et al. [50] and M. Dyck et al. [51] the isoelectric point is 7.4. Based to an isoelectric point of 7.9, NPY should have a net positive charge with a possible localized negative charge. Then, we anticipated an enhanced electrode sensitivity when a negative charge was applied to the working electrode to promote the adsorption of NPY molecules to the negatively charged ssDNA Apts. Because of the dichotomy found in the literature with the isoelectric point of NPY, we opted to test both negative and positive potentials, thereby addressing all possibilities. To assess the potential's influence on biosensor sensitivity, experiments were conducted at -0.4, 0.0, 0.4, and 0.8 V vs. Ag|AgCl. Lower potentials are hypothesized to facilitate NPY adsorption onto the electrode surface, thereby encouraging Apt-NPY binding. Conversely, NPY exhibits a reduced affinity for the electrode surface at higher potentials. [52] Additionally, at 0.8 V vs. Ag|AgCl, guanine oxidation on Au electrodes is anticipated. [52,53] Fig. 3 illustrates NPY measurements across these varied potentials, with NPY concentrations ranging from 1 to 1000 pg/mL. The baseline impedance in aCSF without NPY was subtracted

from each concentration's data, allowing for the isolation of NPY's specific adsorption effects on impedance. Given EIS's capacity to measure the convolution of surface processes, deconvolution is essential when examining a particular phenomenon. [54] In this context, NPY's effect on impedance was isolated by subtracting other surface processes occurring in aCSF. Consistent with prior research, [33,34] the analytical signal used was  $-\omega^*Z_{\rm imag}$ , as this parameter correlates with double-layer capacitance [24] following baseline subtraction. Therefore, employing  $-\omega^*Z_{\rm imag}$  facilitates the examination of NPY's specific adsorption to the surface. [55]

Significant variations in behavior were noted at different potentials, particularly when comparing lower potentials (-0.4 V and 0.0 V) to higher ones (0.4 V and 0.8 V). At -0.4 V, the appearance of two time constants, illustrated by two plateaus, was observed, indicating two distinct capacitances. This phenomenon is explained by the presence of two distinct electrode surface areas, each characterized by specific properties. The differentiation is attributed to the specific regions on the sensor where NPY is bound to the Apt, forming a molecular association, and the contrasting regions where the Apt stands alone, devoid of any such binding. The disparities in properties between these two areas contribute to the observed variations in the characteristics of the electrode surface. [56] At the lower potentials of -0.4 V and 0.0 V, the concentration differences exhibited consistency across various frequencies. However, as the potential increased, the  $-\omega^*Z_{imag}$  values showed more pronounced frequency-dependent fluctuations with less apparent plateaus. Particularly at 0.4 V and 0.8 V, the sensitivity of NPY measurements displayed significant variations contingent on frequency. At 0.4 V, the different NPY concentrations mostly overlapped at low frequencies, with an increasing divergence between concentrations at higher frequencies. A distinct linear relationship between the logarithm

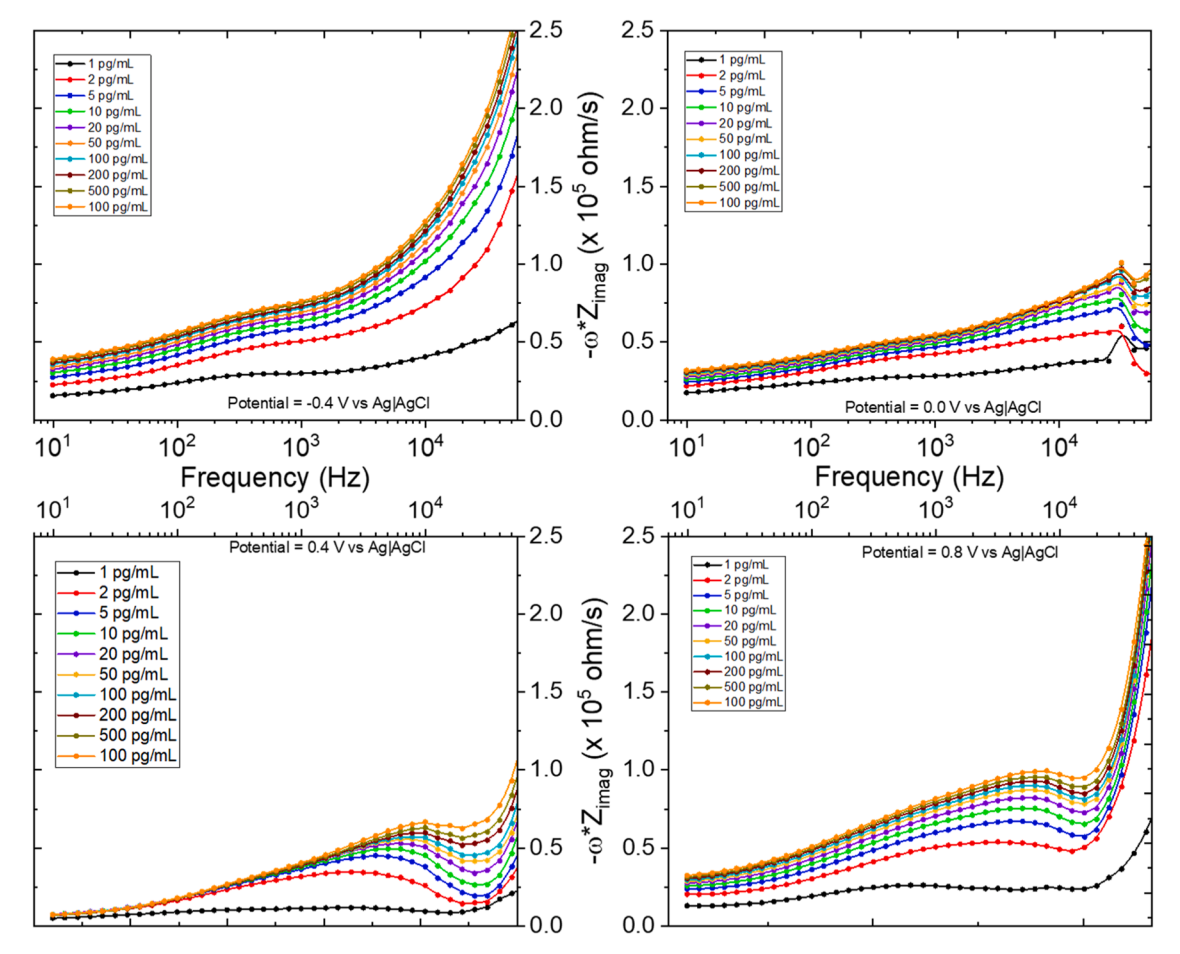


Fig. 3.  $-\omega^*$ Zimag at different potentials of NPY at aptamer-modified Au electrodes.

of concentration and impedance was observed only at high frequencies, from 20 kHz to 50 kHz, for the entire concentration range of 1 to 1000 pg/mL, as depicted in Fig. 4.

### 3.4. Adsorption of NPY on planar AU electrodes

To elucidate the impact of the Apt on the interaction between the target molecule and the sensor surface, thereby influencing sensor sensitivity, calibration curves were constructed plotting  $-\omega Z_{imag}$  against the NPY concentration. As previously mentioned, following background subtraction, the  $-\omega^*Z_{imag}$  component provides insights into the surface capacitance during the interaction. Prior research has demonstrated that  $-\omega^*Z_{imag}$  is indicative of the adsorption capacity of the surface, owing to the correlation between surface capacitance and coverage in microelectrodes. [33,34] In this study, the relationship between  $-\omega^*Z_{imag}$  and surface coverage was explored by testing the linearized form (Eq. (2)) of the Langmuir isotherm equation (Eq. (1)) for our planar electrodes. [57–59]

$$-\omega Z_{imag} = \frac{Q_{Au/apt} K_{Au/apt} C_{NPY}}{1 + K_{Au/apt} C_{NPY}}$$
(1)

$$\frac{C_{NPY}}{-\omega Z_{imag}} = \frac{1}{Q_{Au/apt}} C_{NPY} + \frac{1}{K_{Au/apt} Q_{Au/apt}}$$
(2)

where  $C_{NPY}$  denotes the concentration of NPY at adsorption equilibrium,  $-\omega^* Z_{imag}$  is employed to denote the adsorption capacity of NPY on the modified surface.  $K_{Au/apt}$  signifies the adsorption coefficient of the modified surface, and  $Q_{Au/apt}$  indicates the maximum adsorption capacity when the modified electrode is saturated. Fig. 5 illustrates a plot of  $C_{NPY}/(-\omega^* Z_{imag})$  vs.  $C_{NPY}$  ranging from 1 to 1000 pg/mL, exhibiting a linear fit between 2 and 1000 pg/mL. Notably, the lowest concentration of 1 pg/mL falls outside this linear fitting. Error bars for the Y-axis were included based on n=3 measurements at each concentration point. The analysis revealed that almost all frequencies at each potential could be linearly fitted in this manner, conforming to a Langmuir adsorption isotherm model. The Langmuir isotherm is characterized by adsorption limited to a single molecular layer, depicting the equilibrium between the adsorbate (i.e., NPY) and the adsorbent system (i.e., the Aptmodified Au-coated silicon wafer electrodes). [57–59]

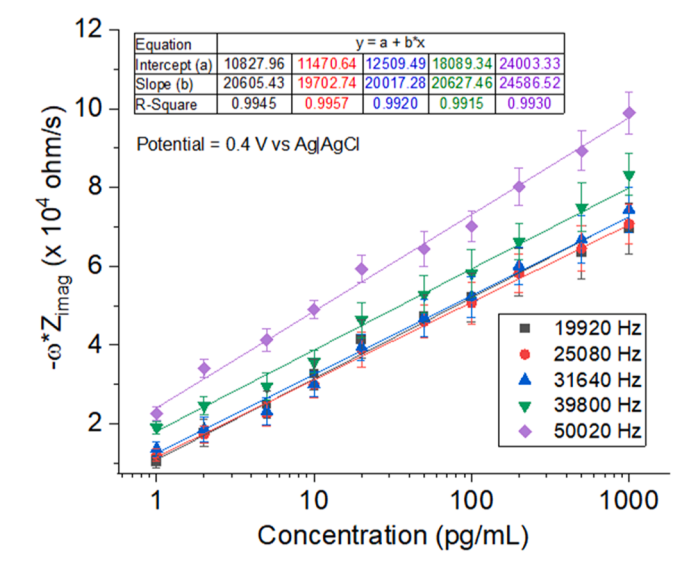


Fig. 4. Measurement of NPY adsorption at high frequencies at 0.4 V vs Ag| AgCl. Linear fittings show the intercept and slope, all with  $R^2 > 0.99$ .

### 3.5. Measurement of NPY

To evaluate how different potentials and frequencies impact the sensitivity of our sensor using EIS, we compared the sensor's response at four tested potentials (-0.4 V, 0.0 V, 0.4 V, and 0.8 V) across three distinct frequencies: low (495.8 Hz), medium (5016 Hz), and high (9984 Hz). This comparison spanned the entire measured range (10 Hz to 10,000 Hz). Initially, the data was filtered to identify the optimal potential and frequency that exhibited significant differences in concentration-response relations. A steeper slope within the significant concentration differences was preferred, indicating greater differentiation between concentrations, thereby enhancing measurement sensitivity. All curves demonstrated a robust linear correlation down to 20 pg/mL when plotted against Log C<sub>NPY</sub>. While it is possible to calculate a detection limit of 0.1 pg/mL using 3.3 times the slope divided by the standard deviation, the dynamic range constrains the quantification to fall within the range of 20 to 1000 pg/mL. Continuous surface processes such as biofouling due to adsorption at the electrode surface were observed at 0.0 V, 0.4 V, and 0.8 V, thereby changing the capacitance with time. These processes altered measurements over time in aCSF, increasing measurement errors. Notably, the sensor's response time, achieved through agitation between measurements, is less than 1 min following our established procedure. Fig. 6A illustrates this by showing three calibration curves at 10 Hz conducted at -0.4 V and 0.8 V vs. Ag AgCl, taken 5 min apart. Notably, the measurement drift was more pronounced at 0.8 V than at -0.4 V, leading to higher data acquisition errors. The lowest error combined with the best slope was observed at low frequencies at a potential of -0.4 V versus Ag/AgCl. Fig. 6B presents the NPY measurements at various concentrations from 1 to 1000 pg/mL, with a linear relationship discernible only between 20 and 1000 pg/mL when plotting  $-\omega^*Z_{imag}$  versus Log  $C_{NPY}$ . For comparative selectivity analysis, the impedance of potentially co-released molecules (DA, NE, and 5-HT) is shown at a concentration of 5 nM, significantly (20×) higher than the maximum NPY concentration tested (1000 pg/mL≈0.24 nM). Moreover, Figure S1 shows complete measurements of NPY ranging from 1 ( $\approx$ 0.24 pM) to 1000 pg/mL ( $\approx$ 0.24 nM), compared with dopamine (DA), norepinephrine (NE), and serotonin (5-HT) at significantly higher concentrations ranging from 1 to 100 nM.

# 3.6. Measurement of npy in aCSF with 10 % hsa

While NPY can be extracted from biological fluids to measure its concentration without effects of non-specific adsorption of other proteins, [60] we evaluated the effect of biofouling on the detection of NPY. We repeated the measurements in a solution of aCSF with 10 % HSA to observe the effect of high protein concentrations. Human CSF and serum have upper concentrations of HSA of 0.045 % (45 mg/dl) [61] and 5.5 % (5.5 g/dl) [61,62], respectively, in adults. Furthermore, the normal concentration of total protein in CSF and serum are about 0.07 % [61,63, 64] and 9 % [62], respectively, in adults. Therefore, in this project, we used a concentration of 10 % HSA to study the effect of protein biofouling on the surface of the electrode. Fig. 7 shows NPY measurements at various concentrations from 1 to 1000 pg/mL, with a linear relationship only between 5 and 500 pg/mL when plotting  $-\omega^*Z_{imag}$ versus Log  $C_{NPY}$ . An increase in capacitance  $(-\omega^*Z_{imag})$ , a shift of linearity to lower concentrations, and an increase in standard deviation was observed in all replicates measured. Because EIS is sensitive to non-specific adsorptions, a change in the impedance was expected while behaving similarly with a different, typically smaller, dynamic range. [12,22]

# 4. Conclusions

In this study, we explored the development of a label-free method for detecting NPY using EIS in aptamer-modified, highly planar electrodes. The biosensors demonstrated selectivity against potentially interfering

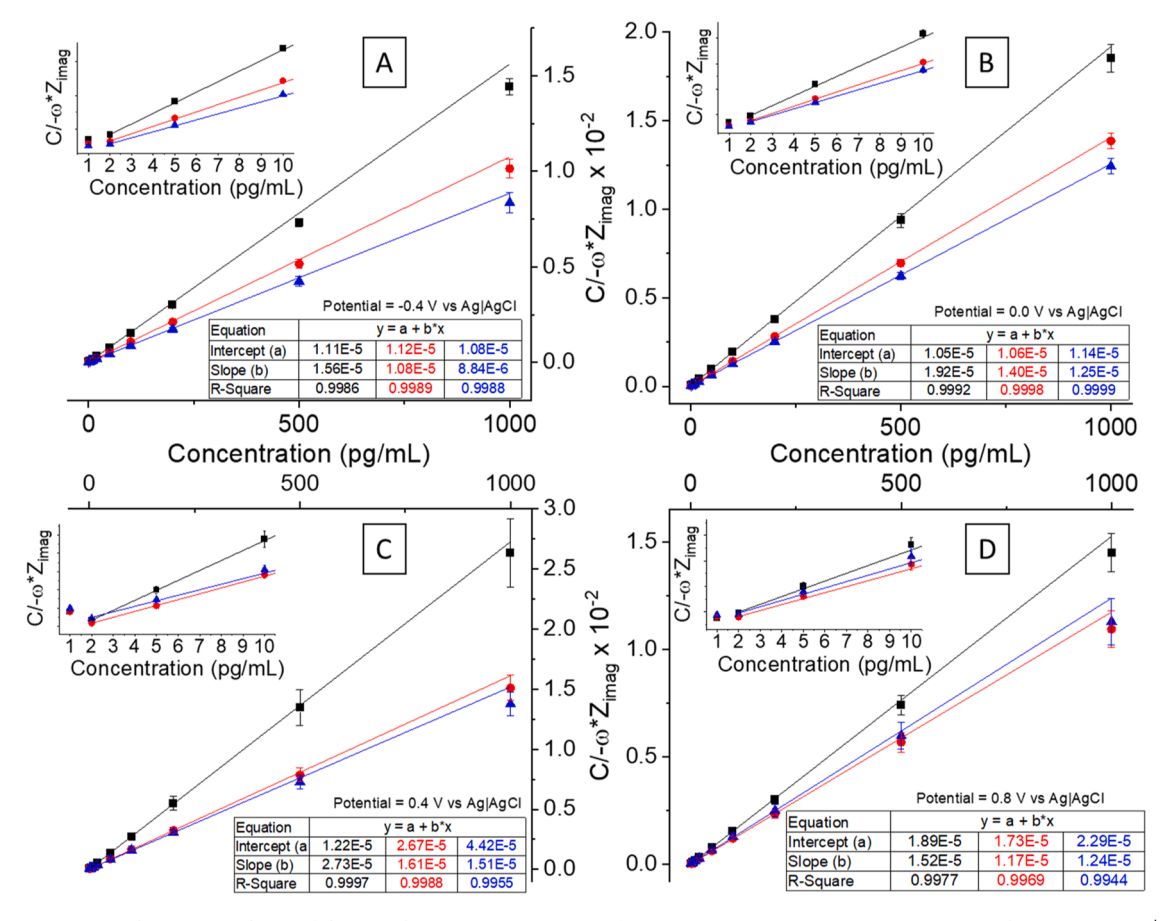


Fig. 5. Langmuir adsorption isotherm of the impedimetric concentrations of NPY at (A) -0.4 V, (B) 0.0 V, (C) 0.4 V, and (D) 0.8 V vs Ag|AgCl.

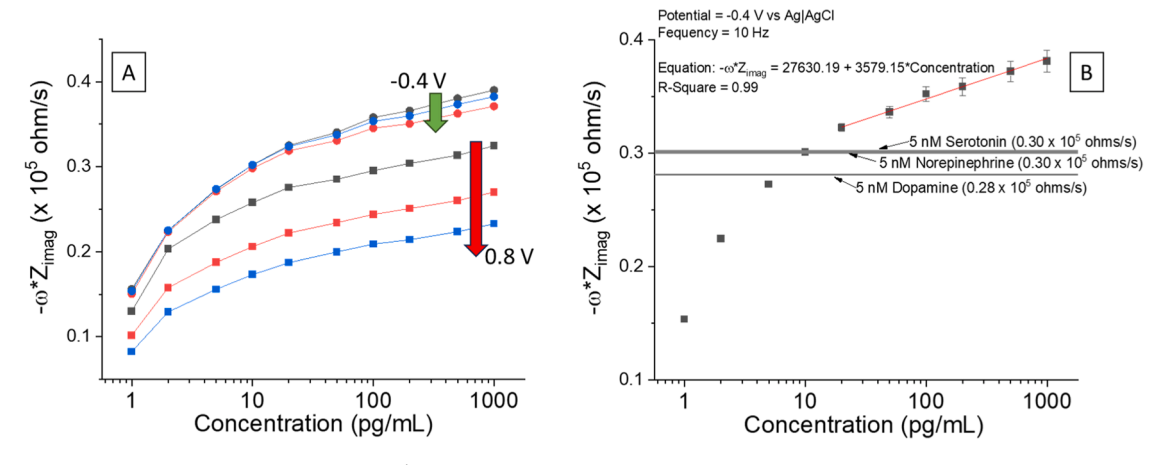


Fig. 6. (A) Drift at -0.4 V (circles) and 0.8 V (squares) vs Ag|AgCl in three measurements taken 5 min apart. (B) NPY measurements at different concentrations from 1 to 1000 pg/mL with a linear relationship between 20 and 1000 pg/mL when plotted as  $-\omega^*Z_{imag}$  vs Log  $C_{NPY}$ . For comparison, measurements of 5 nM of DA, NE, and 5-HT is shown as horizontal lines.

molecules such as DA, NE, and 5-HT, even in scenarios where these molecules were present in a 20-to-1 concentration ratio compared to NPY. This indicates that surface adsorption is a critical factor in molecule detection. We advocated using  $-\omega^*Z_{imag}$  as the analytical signal for NPY measurement, owing to its correlation with both capacitance and adsorption phenomena. Utilizing  $-\omega^*Z_{imag}$ , we proposed that the adsorption of NPY on aptamer-modified planar electrodes adheres to the Langmuir isotherm model. This finding contrasts with previously reported results, which indicated that microelectrodes follow the Freundlich isotherm model. Our findings revealed that, while NPY

adsorption can be detected at concentrations as low as 2 pg/mL, a linear relationship between  $-\omega^*Z_{imag}$  and Log  $C_{NPY}$  allows quantifying NPY concentrations starting from 20 pg/mL if NPY is extracted. In aCSF with 10 % HSA, we found a smaller dynamic range with linearity shifted to as low as 5 pg/mL and a lower upper limit of 500 pg/mL due to the nonspecific adsorption of HSA. The optimal conditions for our biosensor were determined to be using a potential of -0.4~V vs Ag|AgCl at low frequencies such as 10 Hz.

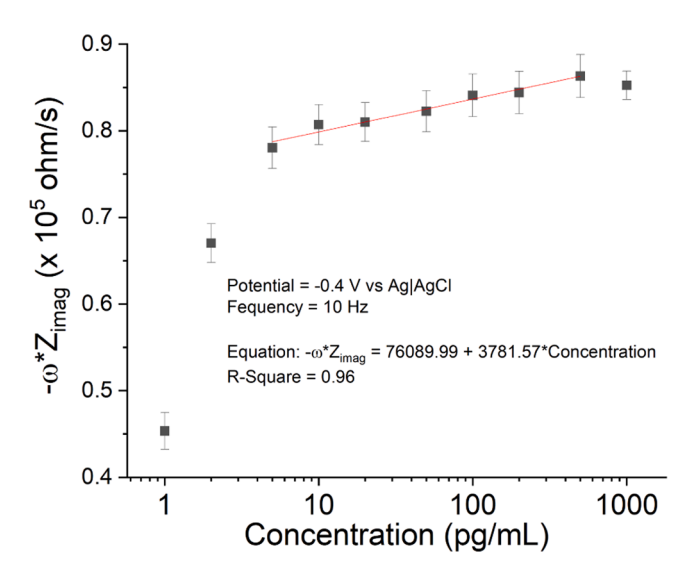


Fig. 7. NPY measurements at different concentrations from 1 to 1000 pg/mL in aCSF with 10 % HSA showing a linear relationship between 5 and 500 pg/mL when plotted as  $-\omega^* Z_{imag}$  vs Log  $C_{NPY}$ .

### CRediT authorship contribution statement

Luis López: Writing – review & editing, Writing – original draft, Investigation, Formal analysis. Lyza M. Martínez: Investigation. Jaileen R. Caicedo: Investigation. Lauren Fernández-Vega: Writing – review & editing, Conceptualization. Lisandro Cunci: Writing – review & editing, Supervision, Conceptualization, Formal analysis, Funding acquisition, Project administration.

# Declaration of competing interest

The authors declare that they have noono known competing financial interests or personal relationships that could have appeared to influence the work reported in this paper.

# Data availability

Data will be made available on request.

# Acknowledgments

This work was supported by the National Institute of Mental Health under grant number 1R21 MH129037 and the National Science Foundation under award numbers 1827622 and 1849243. Student L. L. acknowledges the National Aeronautics and Space Administration Cooperative Agreement No. 80NSSC20M0052 (Puerto Rico Space Grant Consortium). This content is only the responsibility of the authors. It does not necessarily represent the official views of the National Institutes of Health, the National Science Foundation, or the National Aeronautics and Space Administration.

### Supplementary materials

Supplementary material associated with this article can be found, in the online version, at doi:10.1016/j.electacta.2024.144243.

# References

 I. Álvarez-Martos, A. Møller, E.E. Ferapontova, Dopamine binding and analysis in undiluted human serum and blood by the RNA-aptamer electrode, ACS Chem. Neurosci. 10 (2019) 1706–1715, https://doi.org/10.1021/ acschemneuro.8b00616.

- [2] Y. Liu, J. Canoura, O. Alkhamis, Y. Xiao, Immobilization strategies for enhancing sensitivity of electrochemical aptamer-based sensors, ACS Appl. Mater. Interfaces 13 (2021) 9491–9499, https://doi.org/10.1021/acsami.0c20707.
- [3] R. Li, X. Li, L. Su, H. Qi, X. Yue, H. Qi, Label-free electrochemical aptasensor for the determination of serotonin, Electroanalysis 34 (2022) 1048–1053, https://doi.org/ 10.1002/elan.202100373.
- [4] E.E. Ferapontova, K.V. Gothelf, Optimization of the electrochemical RNA-aptamer based biosensor for theophylline by using a methylene blue redox label, Electroanalysis 21 (2009) 1261–1266, https://doi.org/10.1002/elan.200804558.
- [5] M.E. Weese-Myers, A.E. Ross, Electrochemical characterization of 17β-estradiol with fast-scan cyclic voltammetry, Electroanalysis 35 (2023), https://doi.org/ 10.1002/elan.202200560
- [6] I. Álvarez-Martos, E.E. Ferapontova, Electrocatalytic discrimination between dopamine and norepinephrine at graphite and basal plane HOPG electrodes, Electroanalysis 30 (2018) 1082–1090, https://doi.org/10.1002/elan.20170083
- [7] A.M. Downs, J. Gerson, K.L. Ploense, K.W. Plaxco, P. Dauphin-Ducharme, Subsecond-Resolved molecular measurements using electrochemical phase interrogation of aptamer-based sensors, Anal. Chem. 92 (2020) 14063–14068, https://doi.org/10.1021/acs.analchem.0c03109.
- [8] A. İdili, J. Gerson, C. Parolo, T. Kippin, K.W. Plaxco, An electrochemical aptamer-based sensor for the rapid and convenient measurement of tryptophan, Anal. Bioanal. Chem. 411 (2019) 4629–4635, https://doi.org/10.1007/s00216-019-01645-0.
- [9] Ç.G. Aslan, H.D.Ertugrul Uygun, Z.O. Uygun, N.G. Ünal, Y. Akcay, Non-invasive detection of Crohn's Disease with label-free detection of calprotectin by impedimetric aptasensor, Electroanalysis 35 (2023), https://doi.org/10.1002/ elan\_202300119
- [10] S. Brosel-Oliu, D. Galyamin, N. Abramova, F.X. Muñoz-Pascual, A. Bratov, Impedimetric label-free sensor for specific bacteria endotoxin detection by surface charge registration, Electrochim. Acta 243 (2017) 142–151, https://doi.org/ 10.1016/j.electacta.2017.05.060.
- [11] M.E. Strong, J.R. Richards, M. Torres, C.M. Beck, J.T. La Belle, Faradaic electrochemical impedance spectroscopy for enhanced analyte detection in diagnostics, Biosens. Bioelectron. 177 (2021) 112949, https://doi.org/10.1016/j. bios.2020.112949.
- [12] A. Bogomolova, E. Komarova, K. Reber, T. Gerasimov, O. Yavuz, S. Bhatt, M. Aldissi, Challenges of electrochemical impedance spectroscopy in protein biosensing, Anal. Chem. 81 (2009) 3944–3949, https://doi.org/10.1021/ ac9002358.
- [13] K. DeLaney, A.R. Buchberger, L. Atkinson, S. Gründer, A. Mousley, L. Li, New techniques, applications and perspectives in neuropeptide research, J. Exp. Biol. 221 (2018), https://doi.org/10.1242/jeb.151167.
- [14] J.T. Florman, M.J. Alkema, Co-transmission of neuropeptides and monoamines choreograph the C. elegans escape response, PLoS Genet. 18 (2022) e1010091, https://doi.org/10.1371/journal.pgen.1010091.
- [15] M.A. Cortes, K.M. Corder, L.E. Dobrunz, Differences between adult and adolescent male mice in approach/avoidance and expression of hippocampal NPY in response to acute footshock, Stress 24 (2021) 965–977, https://doi.org/10.1080/ 10253890.2021.1976139.
- [16] B. Beck, Neuropeptide Y in normal eating and in genetic and dietary-induced obesity, Philos. Trans. R. Soc. B Biol. Sci. 361 (2006) 1159–1185, https://doi.org/ 10.1098/rstb.2006.1855.
- [17] E.L. Sabban, L.G. Alaluf, L.I. Serova, Potential of neuropeptide Y for preventing or treating post-traumatic stress disorder, Neuropeptides 56 (2016) 19–24, https:// doi.org/10.1016/j.npep.2015.11.004.
- [18] M.R. Emmett, P.E. Andrén, R.M. Caprioli, Specific molecular mass detection of endogenously released neuropeptides using in vivo microdialysis/mass spectrometry, J. Neurosci. Methods 62 (1995) 141–147, https://doi.org/10.1016/ 0165-0270(95)00070-4.
- [19] J. Chavez, K. Rieger, J.A. Hagen, N. Kelley-Loughnane, Biosensor platforms for biomarker detection: plasmonic aptasensors for detection of Neuropeptide Y, D. Kiehl (Eds.), in: B.M. Cullum, E.S. McLamore (Eds.), Smart Biomedical and Physiological Sensor Technology XVI, SPIE, 2019, p. 14, https://doi.org/10.1117/ 12.2520330.
- [20] M.G. Abdallah, J.A. Buchanan-Vega, K.J. Lee, B.R. Wenner, J.W. Allen, M.S. Allen, S. Gimlin, D. Wawro Weidanz, R. Magnusson, Quantification of neuropeptide Y with picomolar sensitivity enabled by guided-mode resonance biosensors, Sensors 20 (2019) 126, https://doi.org/10.3390/s20010126.
- [21] N.K.M. Churcher, S. Upasham, P. Rice, C.F. Greyling, S. Prasad, Sweat based-multiplexed detection of NPY-cortisol for disease diagnostics and stress management, Electroanalysis 34 (2022) 375–386, https://doi.org/10.1002/elan.202100083
- [22] J.M. Seibold, S.W. Abeykoon, A.E. Ross, R.J. White, Development of an Electrochemical, Aptamer-Based Sensor For Dynamic Detection of Neuropeptide Y, ACS Sensors, 2023, https://doi.org/10.1021/acssensors.3c00855.
- [23] L. López, K. Lozano, J. Cruz, K. Flores, L. Fernández-Vega, L. Cunci, Measurement of neuropeptide Y with molecularly imprinted polypyrrole on carbon fiber microelectrodes, Neuropeptides (2024) 102413, https://doi.org/10.1016/j. npep.2024.102413.
- [24] B. Roehrich, K.K. Leung, J. Gerson, T.E. Kippin, K.W. Plaxco, L. Sepunaru, Calibration-Free, seconds-resolved in vivo molecular measurements using fouriertransform impedance spectroscopy interrogation of electrochemical aptamer sensors, ACS Sens. 8 (2023) 3051–3059, https://doi.org/10.1021/
- [25] G. Dutta, F.C.B. Fernandes, P. Estrela, D. Moschou, P.R. Bueno, Impact of surface roughness on the self-assembling of molecular films onto gold electrodes for label-

- free biosensing applications, Electrochim. Acta 378 (2021) 138137, https://doi.org/10.1016/j.electacta.2021.138137.
- [26] E. Rahbarimehr, H.P. Chao, Z.R. Churcher, S. Slavkovic, Y.A. Kaiyum, P. E. Johnson, P. Dauphin-Ducharme, Finding the lost dissociation constant of electrochemical aptamer-based biosensors, Anal. Chem. 95 (2023) 2229–2237, https://doi.org/10.1021/acs.analchem.2c03566.
- [27] M. Jarczewska, A. Trojan, M. Gagała, E. Malinowska, Studies on the affinity-based biosensors for electrochemical detection of HER2 cancer biomarker, Electroanalysis 31 (2019) 1125–1134, https://doi.org/10.1002/elan.201900041.
- [28] A. Rhouati, J.L. Marty, A. Vasilescu, Electrochemical biosensors combining aptamers and enzymatic activity: challenges and analytical opportunities, Electrochim. Acta 390 (2021) 138863, https://doi.org/10.1016/j. electrata 2021 138863
- [29] R. Wang, J. Di, J. Ma, Z. Ma, Highly sensitive detection of cancer cells by electrochemical impedance spectroscopy, Electrochim. Acta 61 (2012) 179–184, https://doi.org/10.1016/j.electacta.2011.11.112.
- [30] M. Tertis, B. Ciui, M. Suciu, R. Săndulescu, C. Cristea, Label-free electrochemical aptasensor based on gold and polypyrrole nanoparticles for interleukin 6 detection, Electrochim. Acta 258 (2017) 1208–1218, https://doi.org/10.1016/j. electacta.2017.11.176.
- [31] E.E. Ferapontova, Electrochemical analysis of dopamine: perspectives of specific in vivo detection, Electrochim. Acta 245 (2017) 664–671, https://doi.org/10.1016/j. electrocta 2017 05 183
- [32] C.Y. Lai, W.C. Huang, J.H. Weng, L.C. Chen, C.F. Chou, P.K. Wei, Impedimetric aptasensing using a symmetric Randles circuit model, Electrochim. Acta 337 (2020) 135750, https://doi.org/10.1016/j.electacta.2020.135750.
- [33] N. Rivera-Serrano, M. Pagan, J. Colón-Rodríguez, C. Fuster, R. Vélez, J. Almodovar-Faria, C. Jiménez-Rivera, L. Cunci, Static and dynamic measurement of dopamine adsorption in carbon fiber microelectrodes using electrochemical impedance spectroscopy, Anal. Chem. 90 (2018) 2293–2301, https://doi.org/ 10.1021/acs.analchem.7b04692.
- [34] L. López, N. Hernández, J.Reyes Morales, J. Cruz, K. Flores, J. González-Amoretti, V. Rivera, L. Cunci, Measurement of neuropeptide y using aptamer-modified microelectrodes by electrochemical impedance spectroscopy, Anal. Chem. 93 (2021) 973–980, https://doi.org/10.1021/acs.analchem.0c03719.
- [35] Y. Xue, X. Li, H. Li, W. Zhang, Quantifying thiol-gold interactions towards the efficient strength control, Nat. Commun. 5 (2014) 4348, https://doi.org/10.1038/ pseumos5348
- [36] L. Zhou, X. Li, B. Zhu, B. Su, An overview of antifouling strategies for electrochemical analysis, Electroanalysis 34 (2022) 966–975, https://doi.org/ 10.1002/elan.202100406.
- [37] X. Zhang, F. Liao, M. Wang, J. Zhang, B. Xu, L. Zhang, J. Xiong, W. Xiong, Enzyme-free recycling amplification-based sensitive electrochemical thrombin aptasensor, Electroanalysis 33 (2021) 1152–1159, https://doi.org/10.1002/elan.202060496.
- [38] J.J. Skaife, N.L. Abbott, Quantitative characterization of obliquely deposited substrates of gold by atomic force microscopy: influence of substrate topography on anchoring of liquid crystals, Chem. Mater. 11 (1999) 612–623, https://doi.org/ 10.1021/cm9804822
- [39] L. Cunci, M.M. Vargas, R. Cunci, R. Gomez-Moreno, I. Perez, A. Baerga-Ortiz, C. I. Gonzalez, C.R. Cabrera, Real-time detection of telomerase activity in cancer cells using a label-free electrochemical impedimetric biosensing microchip, RSC Adv. 4 (2014) 52357–52365, https://doi.org/10.1039/c4ra09689d.
- [40] Q. Chi, G. Wang, J. Jiang, The persistence length and length per base of single-stranded DNA obtained from fluorescence correlation spectroscopy measurements using mean field theory, Physica A 392 (2013) 1072–1079, https://doi.org/10.1016/j.physa.2012.09.022.
- [41] J. Zhou, J. Rossi, Aptamers as targeted therapeutics: current potential and challenges, Nat. Rev. Drug Discov. 16 (2017) 181–202, https://doi.org/10.1038/ nrd.2016.199.
- [42] D.J. Javier, N. Nitin, M. Levy, A. Ellington, R. Richards-Kortum, Aptamer-targeted gold nanoparticles as molecular-specific contrast agents for reflectance imaging, Bioconjug. Chem. 19 (2008) 1309–1312, https://doi.org/10.1021/bc8001248.
- [43] P. Reich, R. Stoltenburg, B. Strehlitz, D. Frense, D. Beckmann, Development of an impedimetric aptasensor for the detection of staphylococcus aureus, Int. J. Mol. Sci. 18 (2017) 2484, https://doi.org/10.3390/ijms18112484.

- [44] T. Pajkossy, R. Jurczakowski, Electrochemical impedance spectroscopy in interfacial studies, Curr. Opin. Electrochem. 1 (2017) 53–58, https://doi.org/ 10.1016/j.coelec.2017.01.006.
- [45] E.P. Randviir, C.E. Banks, Electrochemical impedance spectroscopy: an overview of bioanalytical applications, Anal. Methods 5 (2013) 1098, https://doi.org/10.1039/ c3av26476a.
- [46] M. Kuphal, C.A. Mills, H. Korri-Youssoufi, J. Samitier, Polymer-based technology platform for robust electrochemical sensing using gold microelectrodes, Sens. Actuators B Chem 161 (2012) 279–284, https://doi.org/10.1016/j. snb.2011.10.032.
- [47] X. Li, L. Shen, D. Zhang, H. Qi, Q. Gao, F. Ma, C. Zhang, Electrochemical impedance spectroscopy for study of aptamer-thrombin interfacial interactions, Biosens. Bioelectron. 23 (2008) 1624–1630, https://doi.org/10.1016/j.bios.2008.01.029.
- [48] N.K. Mintah Churcher, S. Upasham, P. Rice, S. Bhadsavle, S. Prasad, Development of a flexible, sweat-based neuropeptide Y detection platform, RSC Adv. 10 (2020) 23173–23186, https://doi.org/10.1039/D0RA03729J.
- [49] K. Ensing, T. de Boer, N. Schreuder, R.A. de Zeeuw, Separation and identification of neuropeptide Y, two of its fragments and their degradation products using capillary electrophoresis–mass spectrometry, J. Chromatogr. B Biomed. Sci. Appl. 727 (1999) 53–61, https://doi.org/10.1016/S0378-4347(99)00084-5.
- [50] L. Thomas, H.A. Scheidt, A. Bettio, D. Huster, A.G. Beck-Sickinger, K. Arnold, O. Zschörnig, Membrane interaction of neuropeptide Y detected by EPR and NMR spectroscopy, Biochimica et Biophysica Acta (BBA) - Biomembranes 1714 (2005) 103–113, https://doi.org/10.1016/j.bbamem.2005.06.012.
- [51] M. Dyck, M. Lösche, Interaction of the neurotransmitter, neuropeptide Y, with phospholipid membranes: film balance and fluorescence microscopy studies, J. Phys. Chem. B 110 (2006) 22143–22151, https://doi.org/10.1021/jp056697
- [52] E. Paleček, M. Bartošík, Electrochemistry of nucleic acids, Chem. Rev. 112 (2012) 3427–3481, https://doi.org/10.1021/cr200303p.
- [53] E.E. Ferapontova, E. Domínguez, Direct electrochemical oxidation of DNA on polycrystalline gold electrodes, Electroanalysis 15 (2003) 629–634, https://doi. org/10.1002/elan.200390079.
- [54] J.R. Espinosa, M. Galván, A.S. Quiñones, J.L. Ayala, S.M. Durón, Dna biosensor based on double-layer discharge for the detection of hpv type, Sensors 16 (2019) 19, https://doi.org/10.3390/s19183956.
- [55] S.M. Park, J.S. Yoo, Peer reviewed: electrochemical impedance spectroscopy for better electrochemical measurements, Anal. Chem. 75 (2003), https://doi.org/ 10.1021/ac0313973, 455 A-461 A.
- [56] S.E. Creager, T.T. Wooster, A new way of using ac voltammetry to study redox kinetics in electroactive monolayers, Anal. Chem. 70 (1998) 4257–4263, https://doi.org/10.1021/ac9804821.
- [57] A.K. Singh, Nanoparticle ecotoxicology. Engineered Nanoparticles, Elsevier, 2016, pp. 343–450. https://doi.org/10.1016/B978-0-12-801406-6.00008-X.
- [58] M. Brdar, A. Takaci, M. Sciban, D. Rakic, Isotherms for the adsorption of Cu(II) onto lignin: comparison of linear and non-linear methods, Hem. Ind. 66 (2012) 497–503, https://doi.org/10.2298/HEMIND111114003B.
- [59] X. Luo, F. Deng, Nanomaterials For the Removal of Pollutants and Resource Reutilization, Elsevier, 2019, https://doi.org/10.1016/C2017-0-01288-0.
- [60] C. Vocat, M. Dunand, S.A. Hubers, N. Bourdillon, G.P. Millet, N.J. Brown, G. Wuerzner, E. Grouzmann, P.J. Eugster, Quantification of neuropeptide Y and four of its metabolites in human plasma by Micro-UHPLC-MS/MS, Anal. Chem. 92 (2020) 859–866, https://doi.org/10.1021/acs.analchem.9b03505.
- [61] H. Hegen, M. Auer, A. Zeileis, F. Deisenhammer, Upper reference limits for cerebrospinal fluid total protein and albumin quotient based on a large cohort of control patients: implications for increased clinical specificity, CCLM (2016) 54, https://doi.org/10.1515/cclm-2015-0253.
- [62] American Board of Internal Medicine, ABIM Laboratory Test Reference Ranges, 2024, p. 2024. - January, https://www.abim.org/Media/bfijryql/laboratory-refer ence-ranges.pdf. accessed April 6, 2024.
- [63] P.R. Bourque, C.R. McCudden, J. Warman-Chardon, J. Brooks, H. Hegen, F. Deisenhammer, A. Breiner, A survey of cerebrospinal fluid total protein upper limits in canada: time for an update? Can. J. Neurol. Sci. 46 (2019) 283–286, https://doi.org/10.1017/cjn.2019.12.
- [64] A. Breiner, D. Moher, J. Brooks, W. Cheng, H. Hegen, F. Deisenhammer, C. R. McCudden, P.R. Bourque, Adult CSF total protein upper reference limits should be age-partitioned and significantly higher than 0.45g/L: a systematic review, J. Neurol. 266 (2019) 616–624. https://doi.org/10.1007/s00415-018-09174-z.